Shadowing Calculation on Urban Areas from Semantic 3D City Models

Xu, Longxiang; León-Sánchez, Camilo; Agugiaro, Giorgio; Stoter, Jantien

DOI
10.1007/978-3-031-43699-4_2

Publication date
2024

Document Version
Final published version

Published in
Recent Advances in 3D Geoinformation Science

Citation (APA)
Xu, L., León-Sánchez, C., Agugiaro, G., & Stoter, J. (2024). Shadowing Calculation on Urban Areas from Semantic 3D City Models. In T. H. Kolbe, A. Donaubauer, & C. Beil (Eds.), *Recent Advances in 3D Geoinformation Science: Proceedings of the 18th 3D GeoInfo Conference* (pp. 31-47). (Lecture Notes in Geoinformation and Cartography). Springer. https://doi.org/10.1007/978-3-031-43699-4_2

Shadowing Calculation on Urban Areas from Semantic 3D City Models

Longxiang Xu, Camilo León-Sánchez, Giorgio Agugiaro, and Jantien Stoter

Abstract Nowadays, our society is in the transit to adopt more sustainable energy sources to reduce our impact on the environment; one alternative is solar energy. However, this is highly affected by the surroundings, which might cause shadowing effects. In this paper, we present our method to perform shadowing calculations in urban areas using semantic 3D city models, which is split into five sections: Point Grid Generation, Sun-Ray Generation, Nightside Filtering, Bounding Volume Hierarchy and the intersection between the sun rays and the BVH to identify which locations are shadowed at a given moment (epoch). Our tests are performed in Rotterdam's city center, a dense urban area in The Netherlands. Our initial results indicate that the computational time per 100 k grid points fluctuates within 0.2–0.7s.

Keywords Solar potential · 3DCM · Shadows analysis · Raytracing

1 Introduction

Currently, our society faces several energy challenges. Most of the produced energy comes from fossil fuels with the consequence of greenhouse gas emissions. On the other side, there are still hundreds of millions of people that do not have access to electricity.

This article was selected based on the results of a double-blind review of an extended abstract.

L. Xu
Delft University of Technology, Delft, The Netherlands
e-mail: L.Xu-18@student.tudelft.nl

C. León-Sánchez (✉) · G. Agugiaro · J. Stoter
Faculty of Architecture and the Built Environment, Department of Urbanism, 3D Geoinformation group, Delft University of Technology, Julianalaan 134, 2628BL Delft, The Netherlands
e-mail: c.a.leonsanchez@tudelft.nl

G. Agugiaro
e-mail: g.agugiaro@tudelft.nl

J. Stoter
e-mail: j.e.stoter@tudelft.nl

T. H. Kolbe et al. (eds.), *Recent Advances in 3D Geoinformation Science*, Lecture Notes in Geoinformation and Cartography, https://doi.org/10.1007/978-3-031-43699-4_2

The United Nations states that by 2050, at least 66% of the world's population will be living in urban areas UN. Population Division (2018). Incorrect quantification of the energy requirements of buildings can result in flawed judgments and misguided strategies for energy supply.

Seeking for clean energy sources is a consequence of the current time Shukla et al. (2022). According to the International Energy Agency (IEA), solar energy and wind power are expected to contribute to 43% of global electricity generation by 2030, an increase from the current 28% IEA (2022). Additionally, the Council of the European Union has reached a political agreement that demands renewable energy sources to comprise 42.5% of Europe's total energy consumption by 2030, with a target of at least 49% renewable energy consumption specifically for buildings, heating, and cooling purposes European Council (2023). In this respect, solar energy plays play a major role as an alternative to meet the growing demand for energy in many countries. However, this energy source is not without challenges such as shadowing, which rapidly decreases the performance of any solar panel, and it is always changing due to the sun movements over the sky.

When solar panels are placed in remote areas with abundant sunlight and generate electricity, significant losses occur during the transmission process. According to the Energy Information Administration (EIA) U.S. Energy Information Administration (2023), losses in power transmission and distribution can amount to 5%, whereas energy losses within urban areas can increase to 50% due to urban morphology Perera et al. (2019). To mitigate energy losses, a decentralized approach of installing solar panels in residential homes can be adopted. Installing photovoltaic systems in residential buildings not only reduces transmission losses and improves energy efficiency but also allows for excess energy generation to be fed back into the urban grid Perera et al. (2019), thereby reducing reliance on fossil fuel-based power generation. However, the decentralized installation of solar panels on rooftops in urban residences may result in fluctuating solar energy output due to dynamic shading caused by cloud cover and surrounding structures.

Shadowing analysis is therefore important in urban planning Palme et al. (2020), especially for solar potential by helping to identify suitable locations in urban areas considering existing structures and future developments; this analysis is relevant for policymakers by encouraging of the population to adopt solar energy while ensuring an efficient utilization of the available resources for a given location.

To perform a shadowing analysis, one needs to consider the geographical location and its surroundings, that is the case for near and far topography, constructions, and vegetation obstacles de Sá et al. (2022). These types of urban objects can be represented by means of semantic 3D city models (3DCM) Agugiaro et al. (2020), which are datasets that allow for a coherent geometrical and semantic representation of urban features in a well-defined data structure.

In this paper, we present the development of a shadowing analysis tool based on 3DCM. Our work consumes the 3DBAG Peters et al. (2022), which is an open dataset containing 3D models of all building in The Netherlands. It is available as downloads in several formats and multiple levels of detail—LoD—(0, 1.2, 1.3, 2.2) Biljecki et al. (2016). Current version consumes the OBJ format.

2 Related Work

In urban contexts, accurately calculating the potential solar irradiance relies on the estimation of shadows during specific times. By integrating solar irradiance and shadowing effect over time, accurate estimates of former can be obtained. Currently, there are three main categories of shadow calculation methods that aims at facilitating solar irradiance estimation: raster-based, viewport, and vector-tracing.

2.1 Raster-Based Methods

Raster-based methods utilize digital elevation models (DEM) or digital surface models (DSM) to represent the urban environment. This approach involves performing shadow calculations in 2.5D, where each location is assigned a single elevation value. The illumination is determined by rasterizing the sun's rays into pixels with elevation and testing for intersections between the rasterized sun rays and the terrain. The method can be also called line-of-sight query Ledoux et al. (2022). Fu and Rich (2002) developed one of the earliest software applications using this method, which has been adopted by ArcGIS Fu and Rich (2002); Hurkmans (2022). Huang et al. (2015) employed this raster method to estimate solar potential in Shanghai, incorporating Graphic Processing Unit (GPU) acceleration Huang et al. (2015). Lukač and Žalik (2013) used a raster DEM to calculate shadows, integrating a variable-resolution grid to capture more details in the DEM for complex urban environments Lukač and Žalik (2013). Raster-based methods are relatively fast and straightforward to implement. However, they are limited to processing 2.5D data, which is a simplified representation of the complex urban environment. These methods therefore struggle to account for intricate vertical structures, and the resolution and accuracy of the DSM/DEM significantly impacts the accuracy and performance.

2.2 Viewport Method

Viewport methods are visualization-based approaches that simulate the view from a prospective shadow-receiving position. The shadowing effect is estimated by the intersection of the sun rays and the surrounding objects within that view.

Tabik et al. (2013) implemented a method to calculate the horizon from the DEM of a shadow-receiving solar panel Tabik et al. (2013). This technique involves determining both a high-resolution near-end horizon and a low-resolution far-end horizon to represent shadows. The method calculates the horizon with an angle resolution of 1°. Calcabrini et al (2019) utilized the sky view factor (SVF) and sun coverage factor (SCF) to estimate shadows Calcabrini et al (2019). SVF represents the portion of the sky visible from the shadow-receiving point, while SCF quantifies the ratio

between shadowed and illuminated times at that location. These factors are derived from skyline profiles obtained by projecting the 3D environment onto 2D shapes at the shadow-receiving position. Stendardo et al. (2020) also employed SVF and SCF calculations using a raster DSM and accelerated the computation with a GPU Stendardo et al. (2020). Zhou et al. (2022) scanned a raster DSM to calculate SVF and SCF. Lan et al. (2021) utilized fisheye street view images to calculate SVF and SCF. Liang et al. (2020) proposed a method that generates cube maps for each shadow-receiving point, where the surrounding environment is projected onto the faces of the cube maps. The shadowing effect is achieved by projecting the sun rays onto the cube maps and testing for intersections. Cube map generation is realized through graphics rendering engines. This straightforward method can be easily implemented using graphics engines and offers high accuracy due to the inherently higher horizontal and vertical angle resolution compared to scanning DSM at intervals.

Viewport methods simulate the view from a shadow-receiving point in a 3D environment. They typically exhibit high accuracy and can incorporate reflective and diffuse irradiance in solar irradiance calculations. However, generating views for all surfaces, whether through DSM scanning or graphic rendering engines, is computationally expensive, especially at a city scale. High-resolution views are necessary for accuracy, but this further intensifies the computational demands. Consequently, viewport methods are more suitable for small-scale simulations and are not applicable for city-scale simulations.

2.3 Vector-Tracing Method

The term "vector tracing method" refers to a technique used to determine shadows by casting sun beams from a surface towards the sun. If the sun's rays are obstructed, the surface is considered to be in shadow. This method relies on testing the intersection between rays and objects. The process of testing whether rays intersect with objects is also known as ray-object intersection test.

Hofierka and Zlocha (2012) developed a method that builds upon raster shadow calculation. They transformed 3D city models into voxels and performed shadow calculations by testing the intersection between sun rays and voxels. This approach involved creating a voxel grid with dynamic resolution to represent different parts of buildings. However, the voxel data model inherently led to redundancy due to a large portion of unoccupied spaces.

The vector tracing method is particularly accurate in complex urban environments since the accuracy of the intersection test remains consistent regardless of scene complexity. However, the computational requirements can be enormous when exhaustively testing the intersection for each ray and each geometric primitive in the scene, such as triangles. Therefore, significant efforts have been made to reduce the number of intersection tests.

Liang et al. (2014) introduced shadow-radius-based culling and view-frustum-based culling, which significantly decreased the number of intersection tests. Wang

et al. (2023) introduced the "neighbourhood shading building surfaces" determination criterion, which includes distance filtering, solar azimuth quadrant filtering, and nightside filtering Wang et al. (2023). These techniques decrease the number of surrounding objects that need to be considered in the intersection test, thereby speeding up the calculation. Hurkmans (2022) utilized an R-tree to partition the scene and accelerate the ray-object intersection. However, the R-tree used in this method is two-dimensional. Similar radius culling methods were also employed.

Although current vector tracing methods have significantly reduced computational requirements, they are implemented with assumptions that sacrifice the accuracy of the vector tracing methods. For example, radius culling methods may result in inaccurate shadow calculations in cases involving high-rise buildings or mountainous terrains. Therefore, the objective of this article is to develop a vector tracing method that does not rely on culling assumptions while efficiently applying shadow casting.

2.4 Other Methods

There are also other methods for shadow calculation available, such as polygon clipping, which involves projecting the polygon surfaces of the surroundings onto the shadow receiving surfaces in the direction of the sun ray Viana-Fons et al. (2020); Zhu et al. (2020). Another method is pixel counting, where a graphics rendering engine is used to render an image at the vantage point representing the sun location to observe the shadow receiving surface. The visible surfaces are illuminated, while the others are considered shadowed Jones and Greenberg (2011). Robledo et al. (2019) utilized graphics engine and determines if a surface is shadowed based on its image z-coordinate. Objects that are closer to the point of view will have a lower z-coordinate. If the shadow receiving surface does not have the smallest z-value in the pixel, it is considered shadowed.

The polygon clipping method is not capable of effectively handling complex city environments due to its limitations in modelling small geometric variations. On the other hand, while pixel counting methods offer high accuracy, they suffer from the same drawback as the viewport method, which requires the graphic engine to exhaustively render different views to determine the shading effect on all surfaces. In the context of a city-scale application, setting up the camera position, rendering fineness, depth of field, and other render options necessitate careful fine-tuning to strike a balance between efficiency and accuracy. Consequently, these two methods are unsuitable for accurately calculating shadows at the city scale.

3 Method

The workflow diagram depicting our process of shadow analysis is presented in Fig. 1. The computation of shadowing effects for a given region involves five key

steps. First, the generation of a point grid on the surfaces of buildings, serving as location samples of the surfaces on which the shadow effect will be calculated. Second, the lines that represent the sun rays are generated with the grid points as starting point and the direction of the sunlight as the ray direction after that we calculate the nightside filtering to exclude from the analysis those points located in surfaces that are opposite to the sun location since this already indicate that they are shadowed. Third, Bounding Volume Hierarchy (BVH) Meister et al. (2021) are reconstructed to efficiently store the city's geometries. Finally, an intersection test is performed between the sun rays and the BVH. The outcome of the intersection tests determines whether the corresponding point's surface is in the shadow at a given epoch.

3.1 Point Grid Generation

Our implementation uses the triangular meshes stored in obj files. We produce a point grid over the building surfaces to locate the samples for shadowing calculation. We use the barycentric coordinates of the input triangles to generate its point grid to

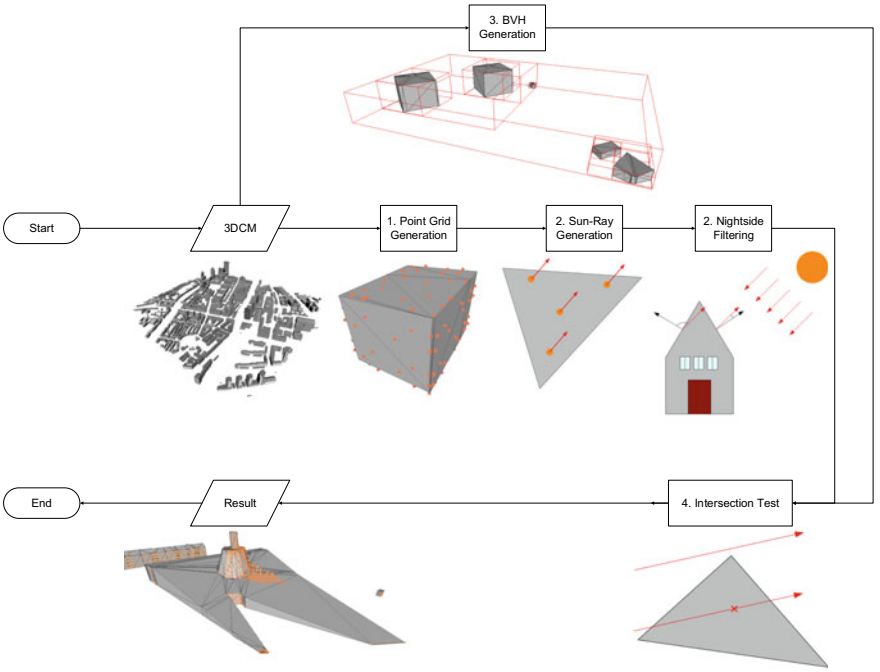

Fig. 1 General workflow of the implemented method

guarantee that point(seconds) are on the triangle's plane. We also add the constraint that the sum of all coefficients of the vector that define the point location is equal to 1 ($w_0 + w_1 + w_2 = 1$) to ensure that each point lies inside the triangle. The adoption of barycentric coordinates and recursive splitting can also handle the situation of sliver triangles and small triangles while uniform spacing will result in undersampling.

The calculation of the point grid for a given triangle and the subsequence division of big triangles into smaller ones consists of the following steps: Figure 2 shows a sketch of the process.

1. Calculate the area of the triangle.
2. Calculate the number of grid's points needed based on 1. (One point per given a defined threshold by the user).
3. Calculate the number of splits needed based on 2.
4. Split the triangle recursively by linking mid points of the bigger triangle edges.
5. Calculate the barycentre of the split triangles.

To ensure uniform samples and full coverage of sliver triangles, an additional constraint is added: When the triangle is sliver, one more split will occur in the corner of acute angle. This constraint mitigates the degenerate case of the method that point grid sampled is uniform in one axis while cluttered in another axis. Figure 4 shows the result of the implementation of this constraint.

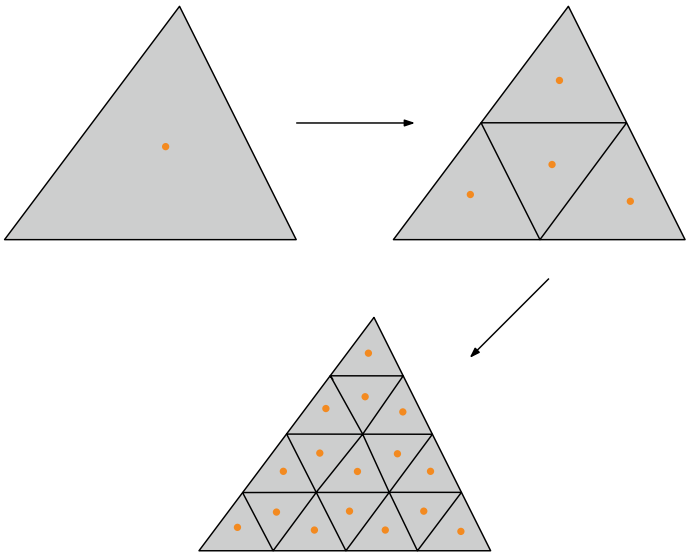

Fig. 2 Illustration of point grid generation

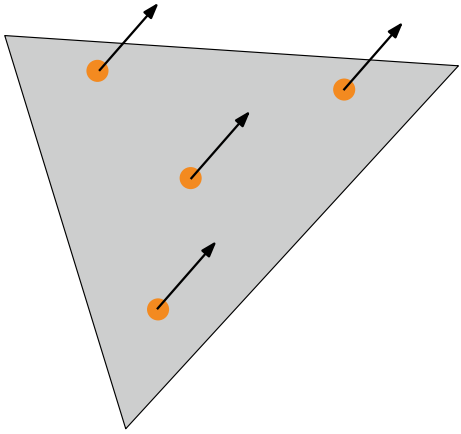

Fig. 3 The illustration of Sun rays generated from point grid on a surface

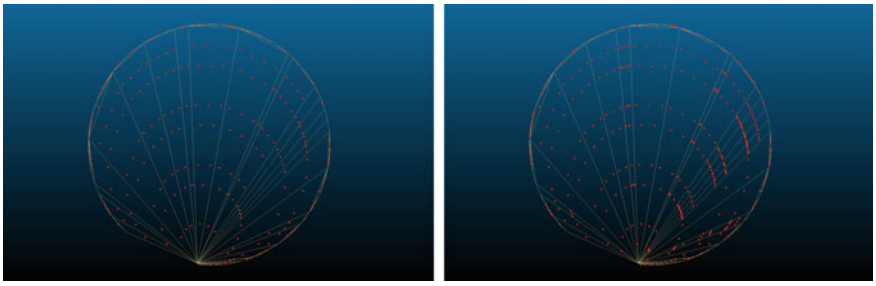

Fig. 4 Comparison of point grid on sliver triangles with (right) and without (left) constraint. Notice there are closer samples covering the acute angle with the constraint. And grid points are spread more evenly across the long axis of the triangles

3.2 Sun Ray Generation with Nightside Filtering

Sun rays are an essential element in shadowing calculations. A ray can be defined by its origin and direction. The location of each point in the previously created grid is used as the starting point to reconstruct the ray and its direction is set to be the vector pointing to the sun as shown in Fig. 3. By this approach, we can test, if the ray originating from the surface will hit any of the surrounding building surfaces. The rays that hit any surface will indicate that its origin (the corresponding grid point) is shadowed.

In this phase of the process, the Nightside Filtering methodology proposed by Wang et al. (2023) is applied to eliminate sun rays that are inevitably incident on surfaces due to self-shadowing. This strategy significantly minimizes the requirement for additional intersection tests. The phenomenon of self-shadowing can be identified by examining the angle between the orientation of the surface and the direction of the

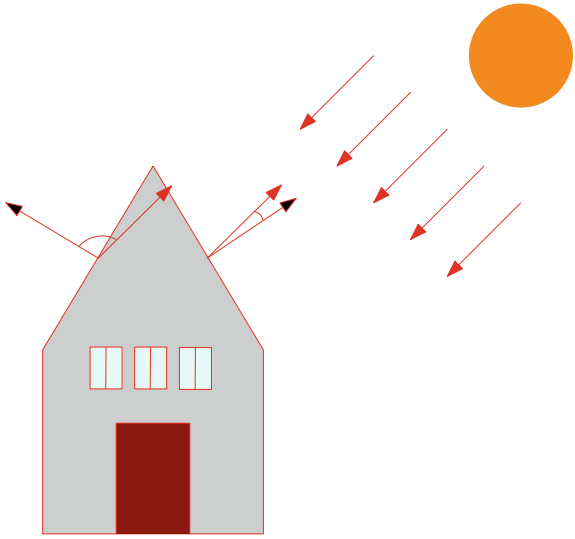

Fig. 5 The illustration of nightside filtering. The black arrow represents the surface normal, and the red arrow represents the sun ray direction

sun ray. When the angle exceeds 90 degrees, self-shadowing is present, eliminating the need for further intersection tests. The respective conditions can be mathematically formulated as:

$$\begin{cases} \mathbf{d} \cdot \mathbf{n} < 0, & \text{self-shadowing occurs (angle} \geq 90^\circ) \\ \mathbf{d} \cdot \mathbf{n} \geq 0, & \text{no self-shadowing (angle} < 90^\circ) \end{cases} \tag{1}$$

In these expressions, $\mathbf{d}$ and $\mathbf{n}$ denote the direction of the sun ray and the surface normal, respectively. It is crucial to note that, in the context of this study, the sun ray's direction originates from the grid point, which is the surface. Consequently, the direction of the sun ray is the inverse of the actual direction. This process is illustrated in Fig. 5.

3.3 Constructing the Bounding Volume Hierarchy

We use the Bounding Volume Hierarchy tree-like acceleration structure to speed-up the sun ray traced rendering Meister et al. (2021). The root node of the BVH tree represents the Axis Aligned Bounding Box (AABB) of the whole scene, then triangles are recursively partitioned into two different groups that contain the same number of triangles. An example of BVH is shown in Fig. 6.

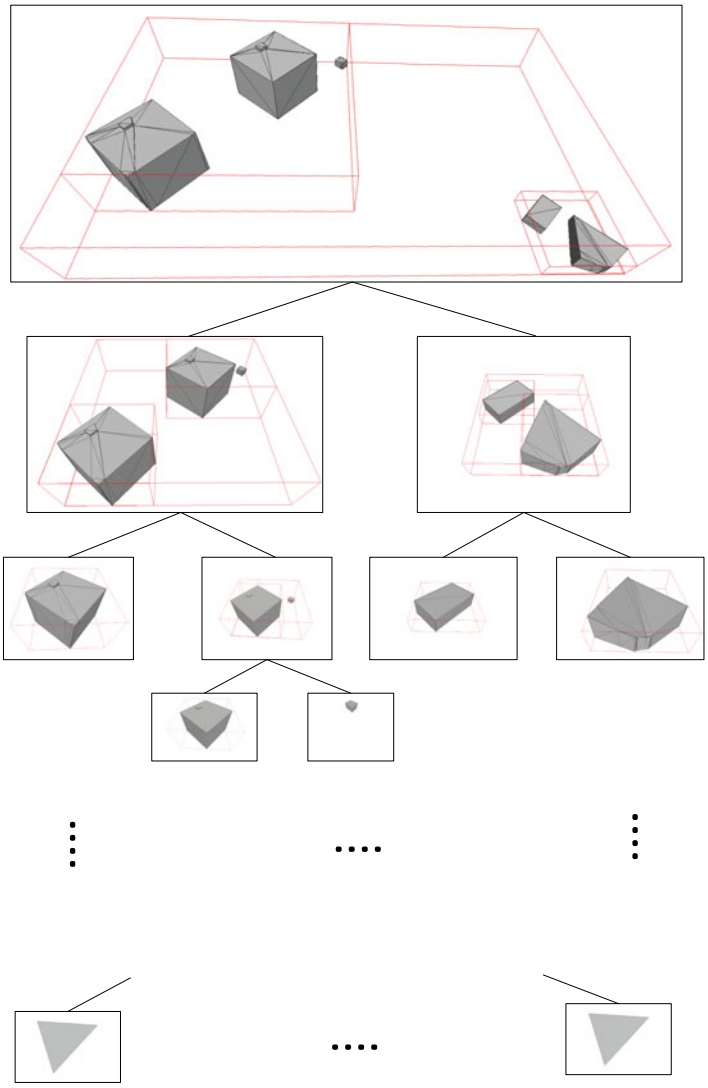

Fig. 6 Illustration of the BVH. Note that the leaf nodes are triangles

3.4 Intersection Test

The tests are applied to each ray and the BVH. Before the intersection test, night-side filtering will be carried out. During this step, the orientation of the sun on the surface, whether it is facing towards or away from the surface, will be determined. Surfaces that are oriented away from the sun (associated sun rays) will be identi-

fied as shadowed and will not undergo any further intersection testing. In the case of parent nodes, further intersection tests are applied on its children's nodes. Since only leaf-nodes are triangles, most of the tests are of the ray-box intersection type, which is computationally less complex compared to ray-triangle intersection tests. Additionally, due to the binary tree structure, the time complexity of the intersection tests decreases from $O(n \cdot m)$ to $O(n \cdot \log_2 m)$, where n represents the number of rays and m represents the number of triangles in the scene.

This hierarchical approach yields significant performance acceleration, particularly for complex scenes covering large areas. When a ray intersects with a triangle, the corresponding origin (grid point) is marked as shadowed.

4 Results

Our method has been implemented in c++. The BVH construction is adopted from the open book Ray Tracing: The Next Week Ray Tracing in One Weekend Book Series (2020). We use an Ubuntu 20.04 distribution over a WSL for Windows 11. The hardware specifications of the computer include a 12th Gen Intel(R) Core (TM) i7-12700H CPU and 32GB RAM.

The experiment on shadow calculation was conducted using the 3D BAG data Peters et al. (2022) of Rotterdam Centrum (see Fig. 7), which encompasses an area of 3.7 km by 3.7 km and includes over 20.000 buildings. The selection of this study area was motivated by its complex urban structure, characterized by numerous tall and densely packed modern buildings, which provided a better reflection of the effectiveness of the algorithm. The tiles corresponding to this area, along with their details, are listed in Table 1.

In this experiment, shadow conditions are computed for the year of 2023. The experiment dates are set on the 1st and 15th of each month, and the corresponding positions of the sun were obtained for these dates. Shadows are calculated at hourly intervals, excluding cases corresponding to the solar altitude below the horizon, which in total, lead to 301 epochs. The setup is intended to evaluate the performance of the model in a real-world scenario.

The experiment involved calculating the shadow for each tile's LoD 2.2 data. For each tile, the shadow analysis is performed for all the surfaces of the buildings contained are computed. Future work will focus on specific surfaces, such as rooftops and building facades, for targeted calculations, leveraging semantic information of 3D city models. Table 2 shows the results of the shadow calculation for the tiles in the study area.

We perform an additional experiment on tile 3340. This tile was designated as the target shadow calculation area, while all surrounding tiles were utilized solely for intersection tests, employing less detailed models (their LoD 1.2 data), thus further reducing the number of potential intersection tests. Specifically, only tile 3340 was sampled (using point grid generation), and all the buildings of tile and the surrounding tiles were constructed into a bounding volume hierarchy. This setup

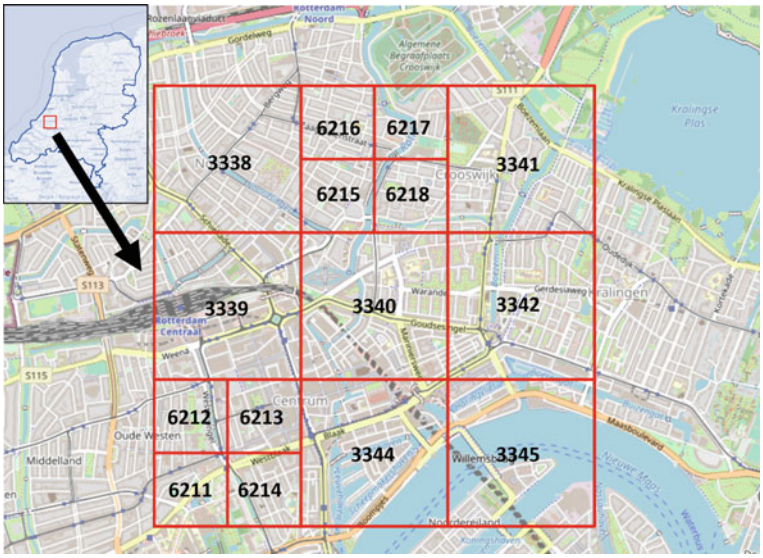

Fig. 7 Study area in Rotterdam, The Netherlands

Table 1 Tile information

Tile	Number of buildings	Number of faces		Extent (m)
		LoD 1.2	LoD 2.2	
3338	1490	111,874	153,834	1251×1253
3339	3347	269,560	391,854	1270×1302
3340	3288	331,432	567,140	1286×1321
3341	568	57,654	91,798	1189×1275
3342	2597	241,951	363,118	1283×1264
3344	1401	200,229	502,830	1339×1354
3345	983	117,122	270,514	1701×1273
6211	1151	117,200	201,096	634×639
6212	825	80,748	128,794	635×576
6213	708	79,964	156,222	669×619
6214	1056	114,448	200,296	644×650
6215	1079	98,149	151,314	644×599
6216	1379	146,891	216,914	638×621
6217	902	103,856	166,366	659×624
6218	1065	96,312	152,625	659×602
Total	21,893	2,167,390	3,714,715	3759×3794

Number of faces correspond to the triangles

Table 2 Experimental results

Tile	PGN (Points)	BVH time (seconds)	Duration (seconds)	D/M (seconds)	D/M/100 k Pts (seconds)
3338	836,540	0.311	619.091	2.056	0.246
3339	2,449,172	0.987	5189.92	17.242	0.704
3340	3,534,632	1.662	5845.02	19.419	0.549
3341	603253	0.235	448.67	1.491	0.247
3342	2,367,691	0.946	4446.05	14.771	0.624
3344	3,904,597	1.292	5800.20	19.536	0.500
3345	2,022,331	0.629	1748.39	5.809	0.287
6211	1,084,487	0.436	2143.96	7.123	0.657
6212	780,436	0.249	1030.72	3.424	0.439
6213	925,722	0.315	916.196	3.044	0.329
6214	1,086,824	0.439	2091.39	6.948	0.639
6215	847,248	0.296	1482.22	4.924	0.581
6216	948,222	0.504	2042.10	6.784	0.715
6217	709,075	0.346	675.816	2.245	0.317
6218	904,768	0.306	1098.04	3.648	0.403

Note PGN represent point grid number, Duration represent the total simulation time, D/M represent simulation time for a single moment, D/M/100 k Pts represent simulation time for a single moment per 100 k grid points

Table 3 Experiment results for tile 3340

Tile	PGN (Points)	BVH time (seconds)	Duration (seconds)	D/M (seconds)	D/M/100 k Pts (seconds)
3340	3,534,632	1.662	5845.02	19.419	0.549
3340 (with buffer tiles)	3,534,632	9.036	7401.05	24.588	0.630
3340 (whole year)	3,534,632	1.519	84812.10	18.931	0.536

Columns and values definitions are the same as the ones in Table 2

aimed to test the scalability of the BVH method. Although the results already indicate that the higher the number of buildings, the longer the duration of the calculation. We have not tested the use of surrounding tiles as obstacles for the location of interest and based on this to analyse whether an increased number of buildings would significantly affect computational costs for the same set of rays. Additionally, this configuration facilitated more accurate shadow calculations for the edge buildings of tile 3340. Table 3 shows the preliminary results of the calculations, the first insights are promising and cover an interesting aspect to deal with adjacent tiles.

Additionally, we performed hourly shadow calculations for each day throughout the entire year 2023, to address the accuracy loss resulting from the bi-monthly time sampling. The hourly calculation facilitates the evaluation of the method's stability at a higher temporal scale.

5 Discussion

The experimental results demonstrate that the proposed method is scalable for computing shadows in urban areas of varying sizes. Without any parallel processing, the average computation time for calculating shadows in a city region, with a spatial extent of 1.3 km $\times$ 1.3 km and thousands of buildings with complex structures at a specific moment, ranges from 1 to 20 s. Based on the theory of $O(\log n)$ for calculating the time complexity of a single ray, adding surrounding shadow-casting surfaces does not significantly increase the computation time for a single ray. Table 3 shows the results for tile 3340 with the inclusion of surrounding tiles in a lower LoD leading to an increase in the total computational time in $\sim$ 26%.

Furthermore, referring to Table 2, the computation time for a single ray does not exhibit a clear positive correlation with the number of shadow-casting surfaces in different tiles. The computation time per 100k grid points fluctuates within the range of 0.2–0.7s. This behaviour might be attributed to the overlapping bounding volume hierarchies. In BVH, the bounding boxes of different BVH nodes may overlap, causing rays to intersect with both child nodes separately. This overlapping of bounding boxes is scene-specific, and thus, the observed results do not violate the $O(\log n)$ theoretical time complexity. In conclusion, employing BVH for partitioning shadow-casting surfaces is an efficient and scalable method for shadow computation.

As a vector tracing method, this approach avoids making assumptions about shadow projections, such as filtering surrounding buildings based on a fixed ratio of shadow projection distance to building height. Through the use of Bounding Volume Hierarchy, this method circumvents the need for such assumptions and accurately handles extreme scenarios in urban environments, including extremely tall buildings, without incurring additional computational overhead. It also implies that the method can also effectively addresses shadow computations in mountainous urban areas by incorporating DTM (Digital Terrain Model) into the BVH. In addition, our sampling strategy ensures the shadowing calculation for small surfaces such as corners and is therefore also potentially suitable for indoor environments.

Furthermore, the current implementation does not utilize parallel processing, indicating significant room for improvement in computational speed. The proposed shadow computation method for urban-scale scenarios exhibits high parallelizability since intersection tests for each ray are independent. With efficient utilization of modern GPU cores (can be as many as several thousands cores in consumer level devices), taking into account the relatively lower single-core performance of GPUs compared to CPUs, the method has the potential to achieve a several-hundred-fold speedup. Moreover, leveraging the specialized RTX core in Nvidia GPUs, specifically designed to accelerate ray-triangle intersection tests, could further enhance the performance of the proposed method after adapting to the RTX core.

Additionally, the current experiment does not utilize semantic information of buildings, it is easily achievable in future code improvements. First use is the distinction between the input obstacles and target elements, the former correspond to all features in the input data-set and the latter correspond to building features and their

corresponding roof and wall surfaces. By recording ray-triangle intersection information, it becomes possible to analyze which buildings occlude specific structures the most severely. Semantics can also facilitate user selection of target computation areas or specific urban objects of interest for calculations i.e., buildings, trees, city furniture, etc.

One limitation of this method is its lack of consideration for diffuse and reflection of light rays. This may restrict its application in accurately calculating solar irradiance.

We expect our implementation to be accurate in complex urban environments; BVH accelerates the intersection tests without relying on any assumption (like buffer distance).

6 Conclusions and Future Work

This work is part of an on-going research about the development of a solar irradiance simulation tool based on semantic 3D city models. Our proposed method works for the calculation of shadows using semantic 3D city models and it is an improvement of existing ones since we use the vector tracing method without relying on culling assumptions. We include the Nightside filtering to optimise the computation to remove all surfaces that their orientation points to the opposite to the sun location.

Future versions of the tool will support CityGML encoding formats (CityGML, CityJSON and the 3DCityDB) to expand its usability. We plan to include parallel computing to speed up the computational time since the steps our method are independent so they can be execute simultaneously.

References

Agugiaro G, González FGG, Cavallo R (2020) The city of tomorrow from ...the data of today. ISPRS Int J Geo-Inf 9(9). ISSN: 22209964. https://doi.org/10.3390/ijgi9090554

Biljecki F, Ledoux H, Stoter J (2016) An improved LOD specification for 3D building models. Comput, Environ Urban Syst 59:25–37. ISSN: 01989715. https://doi.org/10.1016/j.compenvurbsys.2016.04.005

Calcabrini A, Ziar H, Isabella O, Zeman M (2019) A simplified skyline based method for estimating the annual solar energy potential in urban environments. Nat Energy 4(3):206–215. ISSN:2058-7546. https://doi.org/10.1038/s41560-018-0318-6. [Online]. Available: https://www.nature.com/articles/s41560-018-0318-6 (visited on 21 Feb 2023)

de Sá BA, Dezuo T, Ohf D (2022) Shadow modelling algorithm for photovoltaic systems: extended analysis and simulation. J Control, Autom Electr Syst 33(5):1507–1518. ISSN: 2195-3899. https://doi.org/10.1007/s40313-022-00905-2. [Online]. Available: https://doi.org/10.1007/s40313-022-00905-2

European Council (2023) Council and parliament reach provisional deal on renewable energy directive. [Online]. Available: www.consilium.europa.eu/en/press/press-releases/2023/03/30/council-andparliament-reach-provisional-deal-on-renewable-energy-directive/ (visited on 29 May 2023)

Fu P, Rich PM (1 Dec 2002) A geometric solar radiation model with applications in agriculture and forestry. Comput Electr Agric 37(1):25–35. ISSN: 0168-1699. https://doi.org/10.1016/S0168-1699(02)00115-1. [Online]. Available: https://www.sciencedirect.com/science/article/pii/S0168169902001151 (visited on 1 June 2023)

Hofierka J, Zlocha M (2012) A new 3-D solar radiation model for 3-D city models. Trans GIS 16(5):681–690. ISSN: 1467-9671. https://doi.org/10.1111/j.1467-9671.2012.01337.x. [Online]. Available: https://onlinelibrary.wiley.com/doi/abs/10.1111/j.1467-9671.2012.01337.x (visited on 1 June 2023)

Huang Y, Chen Z, Wu B et al (2015) Estimating roof solar energy potential in the downtown area using a GPU-accelerated solar radiation model and airborne LiDAR data. Remote Sens 7(12):17212–17233. Number: 12, Publisher: MultidisciplinaryDigital Publishing Institute, ISSN: 2072-4292. https://doi.org/10.3390/rs71215877. [Online]. Available: https://mdpi.com/2072-4292/7/12/15877 (visited on 1 June 2023)

Hurkmans R (2022) Efficient solar potential estimation of 3D buildings: 3D BAG as use case. MSc Thesis, Delft University of Technology, Delft, NL. [Online]. Available: http://resolver.tudelft.nl/uuid:0d6fe201-5676-48c0-850f-942d1ee9a353

iea (2022) Outlook for energy demand—world energy outlook 2022—analysis. Int Energy Agency. [Online]. Available: https://iea.org/reports/world-energy-outlook-2022/outlook-for-energydemand (visited on 29 May 2023)

Jones NL, Greenberg DP (2011) Fast computation of incident solar radiation from preliminary to final building design. Presented at the building simulation 2011, series. Building simulation, vol 12. IBPSA, pp 577–584. https://doi.org/10.26868/25222708.2011.1271. [Online]. Available: https://publications.ibpsa.org/conference/paper/?id=bs20111271 (visited on 02 June 2023)

Lan H, Gou Z, Xie X (2021) A simplified evaluation method of rooftop solar energy potential based on image semantic segmentation of urban streetscapes. Solar Energy 230:912–924. ISSN: 0038-092X. https://doi.org/10.1016/j.solener.2021.10.085. [Online]. Available: https://www.sciencedirect.com/science/article/pii/S0038092X2100949X (visited on 21 Feb 2023)

Ledoux H, Arroyo Ohori K, Peters R, Pronk M (2022) Computational modelling of terrains. v0.9.2.1. [Online]. Available: https://tudelft3d.github.io/terrainbook/ (visited on 18 May 2023)

Liang J, Gong J, Li W, Ibrahim AN (3 April 2014) A visualization-oriented 3D method for efficient computation of urban solar radiation based on 3D-2D surface mapping. Int J Geogr Inf Sci 28(4):780–798. ISSN: 1365-8816, 1362-3087. https://doi.org/10.1080/13658816.2014.880168. [Online]. Available: http://www.tandfonline.com/doi/abs/10.1080/13658816.2014.880168 (visited on 21 Feb 2023)

Liang J, Gong J, Xie X, Sun J (1 Sept 2020) Solar3D: an open-source tool for estimating solar radiation in urban environments. ISPRS Int J Geo-Inf 9(9):524. ISSN: 2220-9964. https://doi.org/10.3390/ijgi9090524. [Online]. Available: https://mdpi.com/2220-9964/9/9/524 (visited on 21 Feb 2023)

Lukač N, Žalik B (2013) GPU-based roofs solar potential estimation using LiDAR data. Comput Geosci 52:34–41. ISSN: 0098-3004. https://doi.org/10.1016/j.cageo.2012.10.010. [Online]. Available:https://www.sciencedirect.com/science/article/pii/S0098300412003500 (visited on 1 June 2023)

Meister D, Ogaki S, Benthin C, Doyle M, Guthe M, Bittner J (2021) A survey on bounding volume hierarchies for ray tracing. Comput Graph Forum 40:683–712. https://doi.org/10.1111/cgf.142662

Meister D, Ogaki S, Benthin C, Doyle MJ, Guthe M, Bittner J (2021) A survey on bounding volume hierarchies for ray tracing. Comput Graph Forum 40(2):683–712. ISSN: 1467-8659. https://doi.org/10.1111/cgf.142662. [Online]. Available: https://onlinelibrary.wiley.com/doi/abs/10.1111/cgf.142662 (visited on 15 May 2023)

Palme M, Privitera R, Rosa DL (2020) The shading effects of green infrastructure in private residential areas: building performance simulation to support urban planning. Energy Build 229:110–531. ISSN: 0378-7788. https://doi.org/10.1016/j.enbuild.2020.110531. [Online]. Available: https://www.sciencedirect.com/science/article/pii/S0378778820318697

Perera ATD, Coccolo S, Scartezzini J-L (28 Nov 2019) The influence of urban form on the grid integration of renewable energy technologies and distributed energy systems. Sci Rep 9(1):17–756. Number: 1, Publisher: Nature Publishing Group, ISSN: 2045-2322. https://doi.org/10.1038/s41598-019-53653-w. [Online]. Available: https://nature.com/articles/s41598-019-53653-w (visited on 29 May 2023)

Peters R, Dukai B, Vitalis S, van Liempt J, Stoter J (2022) Automated 3D reconstruction of LoD2 and LoD1 models for all 10 million buildings of The Netherlands, English. https://doi.org/10.14358/PERS.21-00032R2

Ray Tracing in One Weekend Book Series (2020) [Online]. Available: https://github.com/RayTracing/raytracing.github.io (visited on 16 May 2023)

Robledo J, Leloux J, Lorenzo E, Gueymard CA (2019) From video games to solar energy: 3D shading simulation for PV using GPU. Solar Energy 193:962–980. ISSN: 0038-092X. https://doi.org/10.1016/j.solener.2019.09.041. [Online]. Available: https://sciencedirect.com/science/article/pii/S0038092X19309168 (visited on 02 June 2023)

Shukla PR, Skea J, Reisinger A, Slade R, Fradera R, Pathak M (eds) (2022) Climate change 2022 mitigation of climate change, ISBN: 978-92-9169-160-9. [Online]. Available: https://www.ipcc.ch/report/ar6/wg3/

Stendardo N, Desthieux G, Abdennadher N, Gallinelli P (2020) GPUenabled shadow casting for solar potential estimation in large urban areas. application to the solar cadaster of greater Geneva. Appl Sci 10(15):5361. ISSN: 2076-3417. https://doi.org/10.3390/app10155361. [Online]. Available: https://www.mdpi.com/2076-3417/10/15/5361 (visited on 21 Feb 2023)

Tabik S, Villegas A, Zapata EL, Romero LF (2013) Optimal tilt and orientation maps: a multi-algorithm approach for heterogeneous multicore-GPU systems. J Supercomputing 66(1):135–147. ISSN: 1573-0484. https://doi.org/10.1007/s11227-013-0891-1. [Online]. Available: https://doi.org/10.1007/s11227-013-0891-1 (visited on 1 June 2023)

UN. Population Division (2018) The world's cities in 2018, United Nations, New York, USA, Technology Report. ISBN: 978-92-1-151549-7, p 34. [On-line]. Available: https://digitallibrary.un.org/record/3799524

US Energy Information Administration (2023) Frequently asked questions (FAQs)—U.S. energy information administration (EIA). [Online]. Available: https://eia.gov/tools/faqs/faq.php (visited on 29 May 2023)

Viana-Fons J, Gonzálvez-Maciá J, Payá J (2020) Development and validation in a 2D-GIS environment of a 3D shadow cast vector-based model on arbitrarily orientated and tilted surfaces. Energy Build 224:110–258. ISSN: 03787788. https://doi.org/10.1016/j.enbuild.2020.110258. [Online]. Available: https://linkinghub.elsevier.com/retrieve/pii/S0378778820303777 (visited on 21 Feb 2023)

Wang X, Zhang X, Zhu S et al (2023) A novel and efficient method for calculating beam shadows on exterior surfaces of buildings in dense urban contexts. Build Environ 229:109–937. ISSN: 0360-1323. https://doi.org/10.1016/j.buildenv.2022.109937. [Online]. Available: https://www.sciencedirect.com/science/article/pii/S0360132322011672 (visited on 26 Feb 2023)

Zhou Y, Verkou M, Zeman M, Ziar H, Isabella O (2022) A comprehensive workflow for high resolution 3D solar photovoltaic potential mapping in dense urban environment: a case study on campus of Delft University of technology. Solar RRL 6(5):2100–478. ISSN: 2367-198X, 2367-198X. https://doi.org/10.1002/solr.202100478. [Online]. Available: https://onlinelibrary.wiley.com/doi/10.1002/solr.202100478 (visited on 21 Feb 2023)

Zhu R, Wong MS, You L et al (2020) The effect of urban morphology on the solar capacity of three-dimensional cities. Renew Energy 153:1111–1126. ISSN: 0960-1481. https://doi.org/10.1016/j.renene.2020.02.050. [Online]. Available: https://sciencedirect.com/science/article/pii/S0960148120302378 (visited on 21 Feb 2023)